

PAPER • OPEN ACCESS

Gate controlled resonant widths in double-bend waveguides: bound states in the continuum

To cite this article: Almas F Sadreev *et al* 2015 *J. Phys.: Condens. Matter* **27** 295303

View the [article online](#) for updates and enhancements.

Related content

- [Spin polarized bound states in the continuum in open Aharonov–Bohm rings with the Rashba spin–orbit interaction](#)
Evgeny N Bulgakov and Almas F Sadreev
- [Tuning of Fano resonances by rotation of continuum: Wave faucet](#)
Almas F. Sadreev, Artem S. Pilipchuk and Alina A. Lyapina
- [S-matrix formalism of transmission through two QBs](#)
Almas F Sadreev, Evgeny N Bulgakov and Ingrid Rotter

Recent citations

- [Bound states in the continuum](#)
Chia Wei Hsu *et al*
- [Mechanical bound state in the continuum for optomechanical microresonators](#)
Yuan Chen *et al*
- [Spin polarized bound states in the continuum in open Aharonov–Bohm rings with the Rashba spin–orbit interaction](#)
Evgeny N Bulgakov and Almas F Sadreev



IOP | ebooks™

Bringing together innovative digital publishing with leading authors from the global scientific community.

Start exploring the collection—download the first chapter of every title for free.

Gate controlled resonant widths in double-bend waveguides: bound states in the continuum

Almas F Sadreev¹, Dmitrii N Maksimov¹ and Artem S Pilipchuk^{1,2}

¹ Kirensky Institute of Physics Siberian Branch of Russian Academy of Sciences, 660036, Krasnoyarsk, Russia

² Siberian Federal University, 660080 Krasnoyarsk, Russia

E-mail: almas@tnp.krasn.ru

Received 16 January 2015, revised 5 May 2015

Accepted for publication 22 May 2015

Published 3 July 2015



Abstract

We consider quantum transmission through double-bend Π - and Z -shaped waveguides controlled by the finger gate potential. Using the effective non-Hermitian Hamiltonian approach we explain the resonances in transmission. We show a difference in transmission in the short waveguides that is the result of different chirality in Z and Π waveguides. We demonstrate that the potential selectively affects the resonant widths resulting in the occurrence of bound states in the continuum.

Keywords: double-bent waveguide, effective non-Hermitian Hamiltonian, bound states in the continuum

(Some figures may appear in colour only in the online journal)

1. Introduction

The effects of bend discontinuities on the transmission in double-bend quantum waveguides have been in the focus of researches for long time [1–9]. A Fano resonance was shown owing to the presence of a single bend [7, 8, 10]. The resonant picture complicates in the double-bend waveguides with the resonance widths and positions dependent on the distance between bends [11, 12]. We believe that these resonances are still not properly understood. One of the aims of the present paper is to give a comprehensive description of resonant effects in double-bend quantum waveguides using the effective Hamiltonian approach [13–18]. The central goal is however to show that the finger gate potential selectively affects resonant widths resulting in the occurrence of zero width resonances. That gives rise to trapping of an electron between the bends or bound state in the continuum (BSC).

The phenomenon of localized state with discrete energy level embedded in the continuum of extended states originally considered in 1929 by von Neumann and Wigner [19] was long time regarded as mathematical curiosity because of certain spatially oscillating potentials. That situation cardinally changed when Friedrich and Wintgen [20] in framework of generic two-level Fano–Anderson model formulated the BSC as a resonant state whose width tends to zero as, at least, one physical parameter varies continuously. Localization of the resonant states of open system, i.e. the BSC is the result of a full destructive interference of two resonance states which occurs for crossing of eigenlevels of the closed system [20–23]. That is accompanied by avoiding crossing of the resonant states one of which transforms into the trapped state with a vanishing width while the second resonant state acquires the maximal resonance width (superradiant state [22]). Recently the BSCs were considered in photonics [24–26] stimulating intensive experimental studies in electromagnetic systems [27–32]. We address the reader to [32, 33] to survey the current state of the art in the area of BSCs.

In the present paper we consider wave transmission through two types of double-bend waveguides, namely

 Content from this work may be used under the terms of the [Creative Commons Attribution 3.0 licence](https://creativecommons.org/licenses/by/3.0/). Any further distribution of this work must maintain attribution to the author(s) and the title of the work, journal citation and DOI.

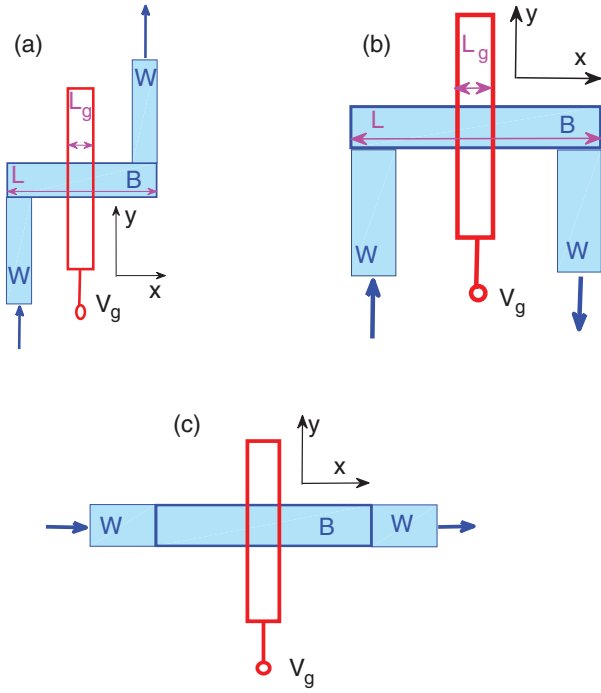


Figure 1. Double-bend waveguides, Z-shaped (a) and Π -shaped (b) with finger gate on the top. Subplot (c) shows a directional waveguide with a finger gate placed across the waveguide axis. Arrows show electron flows.

Z- and Π -shaped quantum waveguides with a finger gate positioned across the wire as shown in figure 1. Each bend of the waveguides has one transmission zero [1, 7, 8] at some energy E_c for the first channel transmission. Therefore the double-bend wire can be considered as a Fabry–Perot resonator (FPR) at the energy E_c . The FPR can trap an electron if the distance between the bends is tuned to the integer number of half-wave lengths. Such a tuning is however hardly experimentally plausible. We propose to employ the finger gate potential in order to effectively tune the distance between the bends. We will show that multiple BSCs related to integer numbers of half wavelengths between the bends occur for positive potential. For a negative potential we will show the BSCs which are close to those considered by Robnik [34]. Although in what follows we consider the electron transmission through the quantum double-bend waveguides the consideration is applicable to microwave transmission of TM waves owing to the equivalence between the Schrödinger equation and the Maxwell equations for planar electromagnetic waveguides. The dielectric slab inserted between the bends of a waveguide could play the role of the finger gate potential.

2. Transmission through double-bend waveguides

The standard technique to reduce the resonant widths in electron transmission through a quantum dot is to implement quantum point contacts. In the present paper we consider a different approach to selectively control the coupling between

the inner states and the propagating states of the waveguides in the layouts shown in figures 1(a) and (b). As shown in figure 1 we split each double-bend waveguide into three parts. The inner part outlined by bold blue line in figure 1 and denoted by ‘B’ plays the role of a bridge between two semi-infinite directional waveguides denoted by ‘W’. The propagating states with the Fermi energy

$$E_F = \pi^2 p^2 + k_p^2, p = 1, 2, 3, \dots \quad (1)$$

in the waveguides are given by

$$\psi_{\pm}(x, y) = \sqrt{\frac{1}{2\pi k_p}} \exp(\pm i k_p y) \phi_p(x), \quad (2)$$

where

$$\phi_p(x) = \sqrt{2} \sin(\pi p x). \quad (3)$$

Here the Fermi energy is measured in terms of $E_0 = \frac{\hbar^2}{2m^*d^2}$, the coordinates are measured in terms of the width of waveguides d and the wave vector k_p is measured in terms of the inverse width of the waveguides. The eigenfunctions of the inner part ‘B’ are given by the following Schrödinger equation

$$\hat{H}_B \psi_{mn}(x, y) = E_{mn} \psi_{mn}(x, y), \quad \hat{H}_B = -\nabla^2 + V_g(x), \quad (4)$$

$$\psi_{mn}(x, y) = \phi_m(x) \psi_n(y), \quad \psi_n(y) = \sqrt{2} \sin(\pi n y), \quad (5)$$

$$E_{mn} = \epsilon_m(V_g) + \pi^2 n^2, \quad (6)$$

$\phi_m(x)$ and ϵ_m are the eigenfunctions and eigenenergies of a quantum particle in an infinitely deep box of width L with the finger gate potential $V_g(x)$ symmetrical in the x -axis. The exact analytical expression for the potential profile $V_g(x)$ was derived in [35]. If, however, the finger gate is close enough to the 2DEG, the potential can be well approximated by a rectangular step-wise function [36] with height V_g and width L_g equal to the width of the gate.

The conductance of double-bend waveguides could be calculated with the use of the effective non-Hermitian Hamiltonian [13–18]

$$\hat{H}_{\text{eff}} = \hat{H}_B - i\pi \hat{W} \hat{W}^\dagger \quad (7)$$

which is the result of projection of the total Hilbert space onto the inner space of the bridge using the Feshbach technique [37, 38]. In this approach the waveguides are coupled to the bridge by the matrix \hat{W} whose elements are the coupling constants of the first channel propagating state (2) with the inner states (5) calculated via overlapping integrals of the form [17, 18, 39]

$$\begin{aligned} W_{m,n} &= \frac{1}{\sqrt{k_1}} \int_0^1 dx \psi_1(x) \frac{\partial \psi_{m,n}(x, y=0, 1)}{\partial y} \\ &= \frac{2\pi n}{\sqrt{k_1}} \int_0^1 dx \psi_1(x) \phi_m(x). \end{aligned} \quad (8)$$

Then the transmission amplitude is given by [13–16, 18]

$$t = -2\pi i \hat{W}^\dagger \frac{1}{\hat{H}_{\text{eff}} - E} \hat{W}. \quad (9)$$

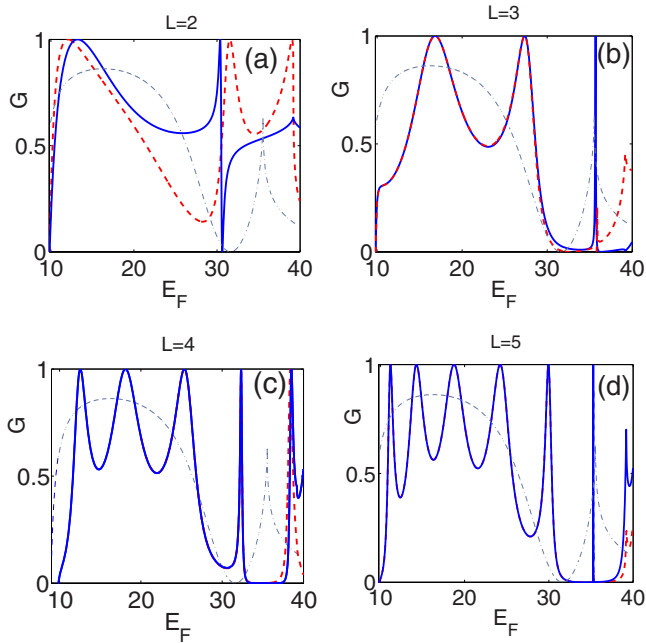


Figure 2. Conductance of double bent Z-shaped waveguide (red dash line) and Π -shaped waveguide (blue solid line) for $V_g = 0$ and four different lengths L . The conductance of the single bent waveguide is shown by green dot–dash line.

Computationally the method of the effective non-Hermitian Hamiltonian becomes efficient when adapted to a discretized form [18, 40] equivalent to the finite-difference approach to the Schrödinger equation that is free from issues of poor convergence [17]. The above approach is equivalent to the technique by Ando [41] that is somewhat less time-consuming and therefore was used in this work for finding scattering and BSC wave functions. We mention in passing that both method yielded the same results for transmission coefficients. In figure 2 we plot the conductance $G = |t|^2$ in the Z-shaped waveguide in comparison to the conductance in the Π -shaped waveguide for $V_g = 0$ for different lengths L .

First, one can observe resonant peaks which become narrower with the growth of L . That observation was reported in [1, 2, 4, 5] however it did not receive a clear explanation. Second, below the threshold of the second channel $E_F = 4\pi^2$ but $E_F > 30$ we see sharp asymmetric Fano resonances where the transmission can be either zero or unit depending on the type of the waveguide. For comparison we presented in figure 2 the conductance of the single bent waveguide by dash–dot line which does not exhibit resonances but has a transmission zero at energy $E_F \approx 31.62$. Third, the conductance in the Z-shaped waveguide differs from the conductance in the Π -shaped waveguide when the second channel of the bridge B participates in the electron transmission. The difference between waveguides tends to zero with the extension of the length L of the bridge. The transmission resonances for energies far below the second channel threshold $E < 4\pi^2$ are typical for the transmission through double barrier structure where peaks of the transmission correspond to standing waves between the barriers. Figure 3 shows the probability distributions which indeed demonstrate standing waves at the transmission resonances.

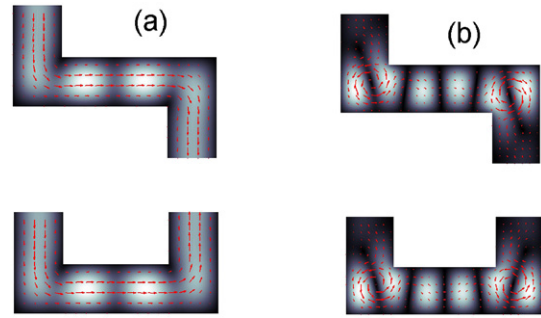


Figure 3. Probability density distributions and current flows (red arrows) in double bent Z- and Π -shaped waveguides for energies $E_F = 18.11$ (a) and $E_F = 32.33$ (b) which correspond to the second and fourth resonant peaks in figure 2 (c) with $L = 4$.

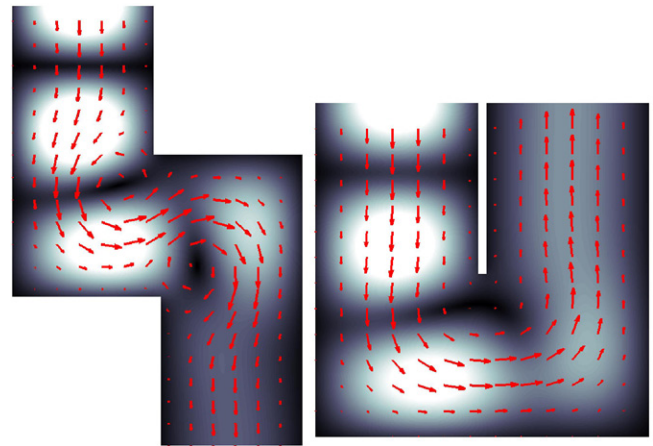


Figure 4. The same as in figure 3 for $L = 2$ and $E_F = 25$.

Figure 3(a) shows that mainly the eigenfunctions $\psi_{m,1}(x, y)$ contribute to the scattering wave function for long waveguides with $L = 4$ with the Fermi energy far from the second channel band edge. In the other words, the waveguides can be considered as one-dimensional in which there is no difference between the chirality sequence of the bends. The current flows demonstrate laminar regime respectively. When the energy is approaching the second channel edge $E = 4\pi^2$ the contribution of the second channel functions $\psi_{m,2}$ becomes relevant giving rise to vortical motion as it was first observed by Berggren and Ji [42] for electron transmission through a single bend waveguide. The direction of current circulation at the vortices depends on the chirality of the bend. Therefore the Π -shaped waveguide with the bends of the same chirality have vortices with the same clockwise or counter-clockwise current circulation while the Z-shaped waveguide with the bends of opposite chirality has vortices of opposite current circulation as seen from figure 3(b). As a result the current flows and respectively the transmission depends on the type of the double-bent waveguide. Figure 4 shows that for the shortest bridge $L = 2$ the current flow is vortical even for energies far from the second channel band edge which gives rise to a difference in conductance for the whole energy band as seen from figure 2(a). In figure 5 we show the first channel conductance for both types of waveguides versus the Fermi energy and the finger gate potential for a long bridge $L = 3$. The waveguides show

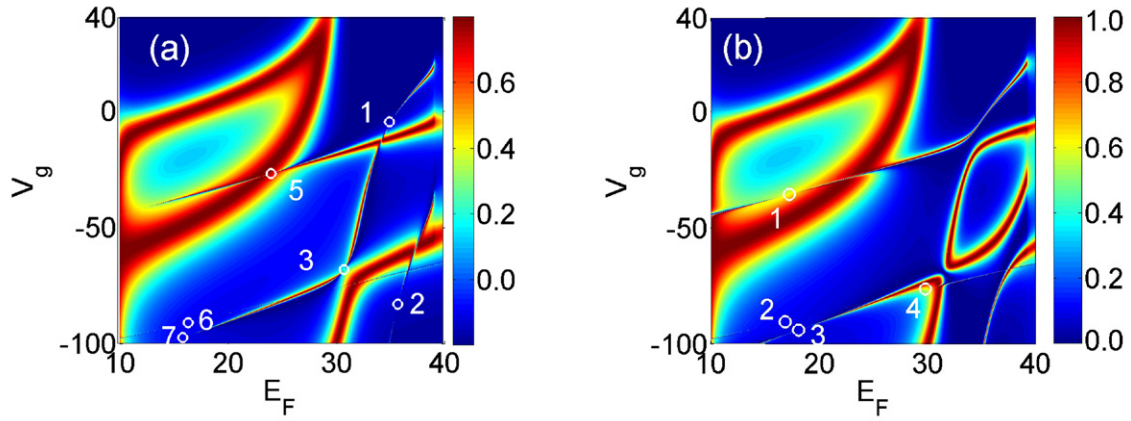


Figure 5. Conductance of double-bent waveguide versus Fermi energy E_F and V_g for Z- (a) and Π -shaped waveguides (b) for $L = 3$. Open circles mark BSC.

generally very similar conductance although with cardinally different pattern of the avoided crossings. As will be shown below that is reflected in the number and types of the BSC which denoted by open white circles in figure 5.

The resonant widths are controlled by the value of the coupling matrix elements (8). Because the longitudinal wave functions $\phi_m(x)$ are normalized to have $L^{1/2}$ in the denominator we obtain that the resonant widths are inversely proportional to L according to equation (7). That observation explains the tendency of narrowing of resonant peaks with the growth of the bridge length L as shown in figure 2. Moreover, that opens an opportunity to control the resonant widths by the potential of the finger gate. This point has a key importance for the BSC and will be considered in the next section.

3. Bound states in the continuum

The complex eigenvalues z of the effective Hamiltonian \hat{H}_{eff} have a simple physical meaning [13, 14, 39]. Their real parts $E_r = \text{Re}(z)$ define the positions of the resonances with the resonance widths given by imaginary parts $\Gamma_r = -2\text{Im}(z)$. In order to find the complex eigenvalues z in case of noticeable radiation shifts it is necessary to solve the fix point equations for the resonance positions [14] $E_r = \text{Re}[z(E_r)]$, $\Gamma_r = \text{Im}[z(E_r)]$. Resonant widths as functions of the finger gate potential V_g show in figure 6 oscillating behavior because the longitudinal wave functions of the bridge $\phi_m(x)$ tend to accumulate their nodal points on the waveguide-bridge interface as the probability distribution is pushed from the central region of the bridge with the growth of the finger gate potential as shown in the inset in figure 7(a). As a result the overlapping integrals

$$J_m = \int_0^1 dx \psi_1(x) \phi_m(x) = \sqrt{2} \int_0^1 dx \sin \pi x \phi_m(x) \quad (10)$$

in the coupling matrix elements in equation (8) behave non monotonically as shown in figure 7(b). Respectively one can see unusual behavior of the resonances shown in inset of figure 6(a). As shown in figure 6(b) further growth of V_g gives rise to a hierarchical trapping of resonances predicted by Rotter and co-authors [43, 44] as a result of the repulsion of complex eigenvalues of the effective Hamiltonian with the

growth of the eigenvalue density. That phenomenon also takes place in Π -shaped waveguides at a different length L .

Next, under variation of the the finger gate potential a unique case can occur when the inverse of matrix $\hat{H}_{\text{eff}} - E$ in equations (9) does not exist, when the determinant $|\hat{H}_{\text{eff}} - E| = 0$. That corresponds to $\text{Im}[z(E_{\text{BSC}})] = 0$ and $E_{\text{BSC}} = \text{Re}[z(E_{\text{BSC}})]$. These equations define the necessary and sufficient condition for the BSC [45, 46] and can be combined into a single equation for the BSC point

$$|H_{\text{eff}}(E_{\text{BSC}}) - E_{\text{BSC}}| = 0. \quad (11)$$

The corresponding eigenfunction of the effective Hamiltonian is the BSC function, respectively. The solution figure 6(c) demonstrates multiple BSCs denoted by red open circles occurring under variation of V_g . An alternative approach to diagnose the BSC is calculating the poles of the S-matrix and finding the condition under which a complex pole tends to the real axis [48–53]. Clearly, as the imaginary part of a pole or a complex eigenvalue tends to zero both methods yield identical results. The BSCs can be also be found in the conductance versus the Fermi energy and the potential V_g as the singular points where full reflection ($G = 0$) meets the full transmission ($G = 1$) [23, 27, 28]. These points are singular due to the collapse of the Fano resonances [47]. In figure 5(a) these points are marked by white circles and enumerated to show corresponding BSC functions in figure 8. The BSC wave function 4 is very similar to the BSC wave function 3 and is not shown in figure 8.

In figure 8 one can see two different types of BSCs. The first three 1–3 are due to the FPR mechanism discussed in the Introduction. The other three BSC functions 5–7 are reminiscent to those considered by Robnik [34] in a directional quantum waveguide with a negative potential V_g shown in figure 1(c). In this case the Schrödinger equation is separable

$$\psi(x, y) = \sin(\pi n y / d) \phi(x) \quad (12)$$

which gives rise to the effectively one-dimensional transmission through a potential well

$$\frac{\partial^2 \phi}{\partial x^2} + [\epsilon - V_g(x)] \psi = 0 \quad (13)$$

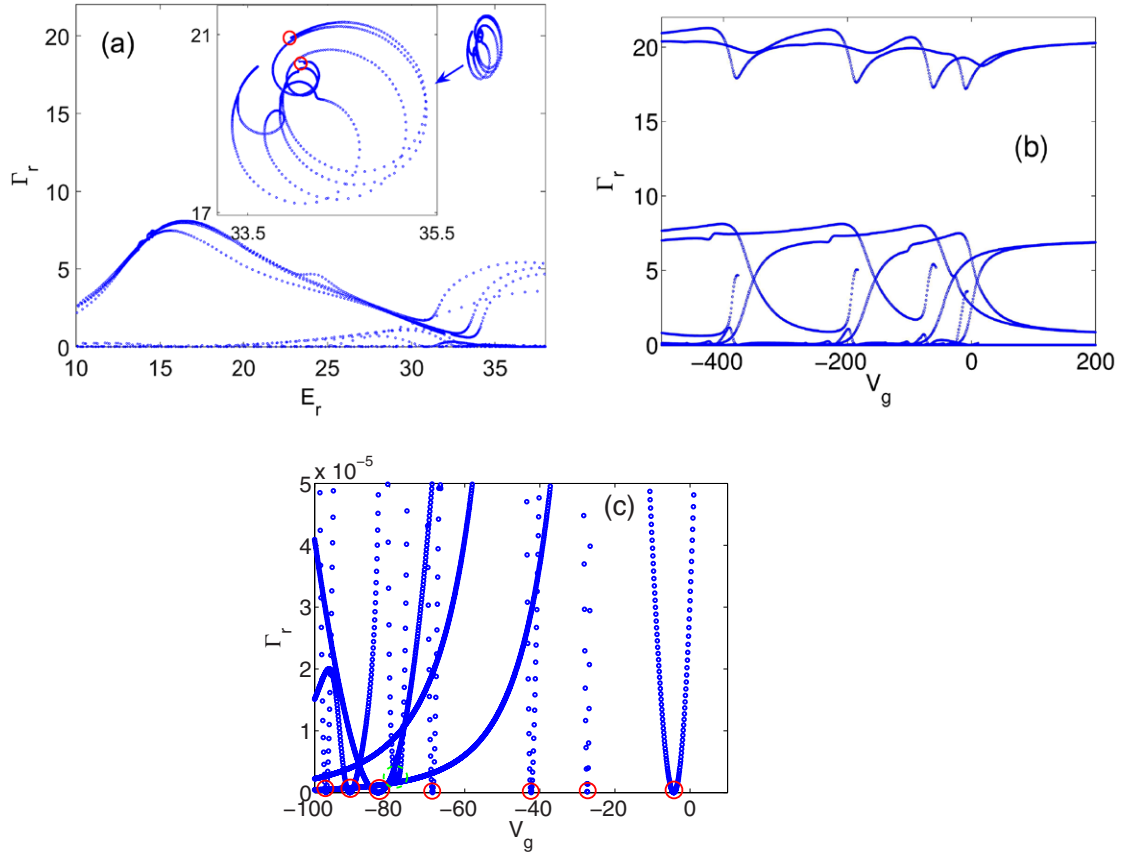


Figure 6. (a) Evolution of resonant positions E_r and resonant widths Γ_r under variation of the finger gate potential V_g for the Z-shaped double bend waveguide $L = 3$. V_g varies in the range $[-500, 200]$. All but two resonant energies grow with the increase of V_g . The evolution starting point $V_g = -500$ for two broad resonances are shown by red circles in the inset. (b) The resonant widths versus V_g . (c) The same as in (b) but zoomed to demonstrate the positions of BSCs. The BSC points are shown by red open circles. A quasi-BSC is shown by a green dashed circle.

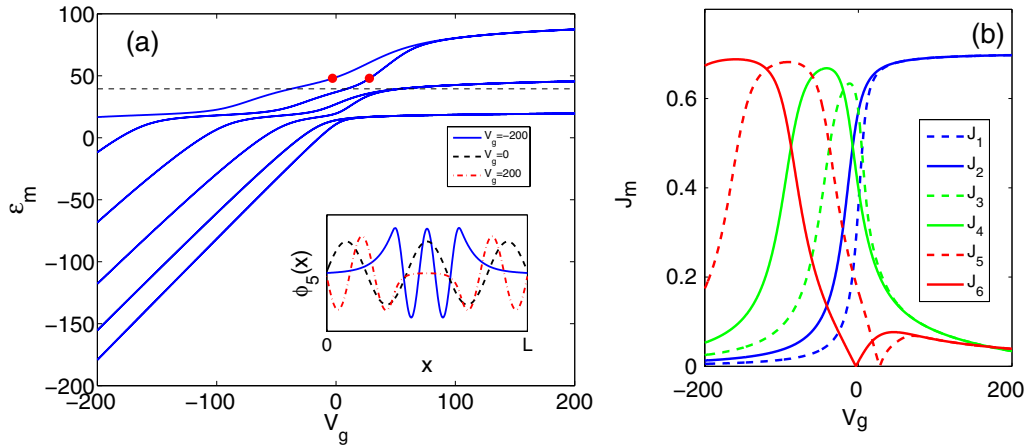


Figure 7. The first six lowest energy levels (a) and overlapping integrals (10) (b) versus V_g . Inset shows wave function $\phi_5(x)$ for $V_g = 0, \pm 200$. The dashed horizontal line in (a) shows the second channel propagation threshold. Red spots indicate the points where the coupling constants J_m equal zero.

where

$$\epsilon = E - \frac{\pi^2 n^2}{d^2}. \quad (14)$$

There are approximately $N = L\sqrt{-V_g}/\pi$ one-dimensional bound states $\phi_m(x)$ with discrete energies ϵ_m in the potential

well with length L_g in terms of the width of the waveguide d and depth V_g for $V_g < 0$ [34]. All bound states with $n = 1$ and $\epsilon_m < 0$ are below the first channel propagation band and therefore are not BSCs. But the bound states with $n = 2, 3 \dots$ and energies $4\pi^2 > \pi^2 n^2 + \epsilon_m$ become BSC because of their orthogonality to the first channel propagation state with $n = 1$.

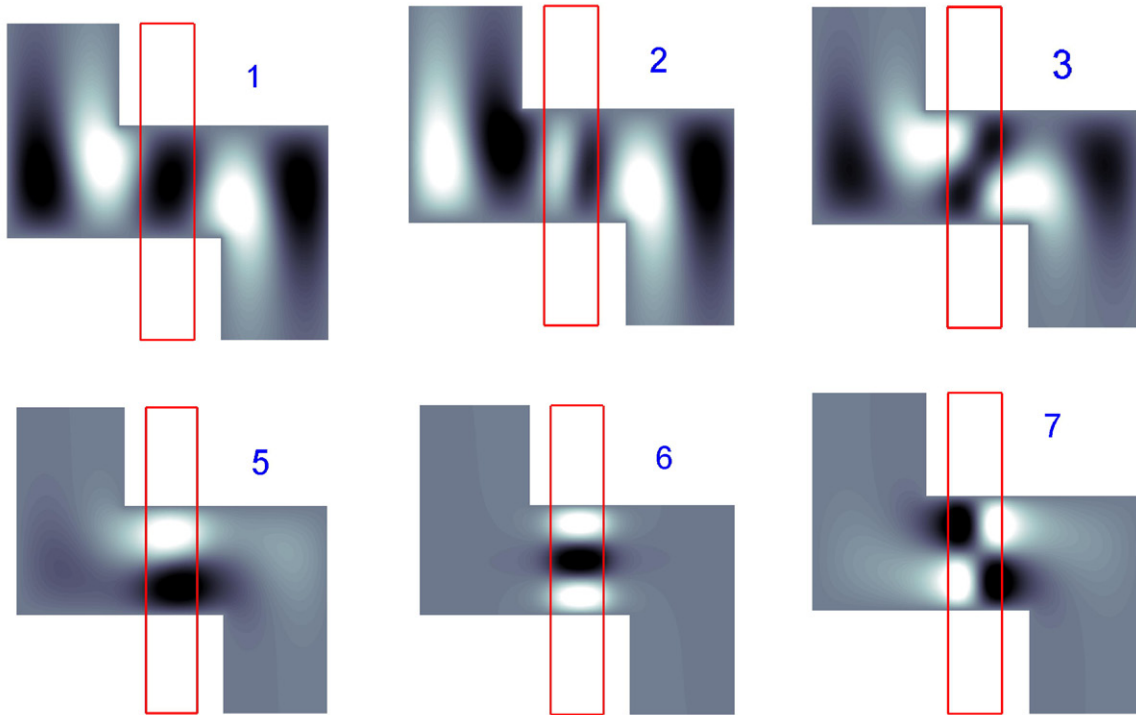


Figure 8. BSC wave functions for the Z-shaped waveguide with $L = 3$ labelled in figure 5(a). (1) $E = 35.066, V_g = -4.8$, (2) $E = 35.845, V_g = -83.11$, (3) $E = 30.8864, V_g = -68.205$, (5) $E = 24.15, V_g = -26.98$, (6) $E = 16.49, V_g = -90.98$, and (7) $E = 16.023, V_g = -97.37$.

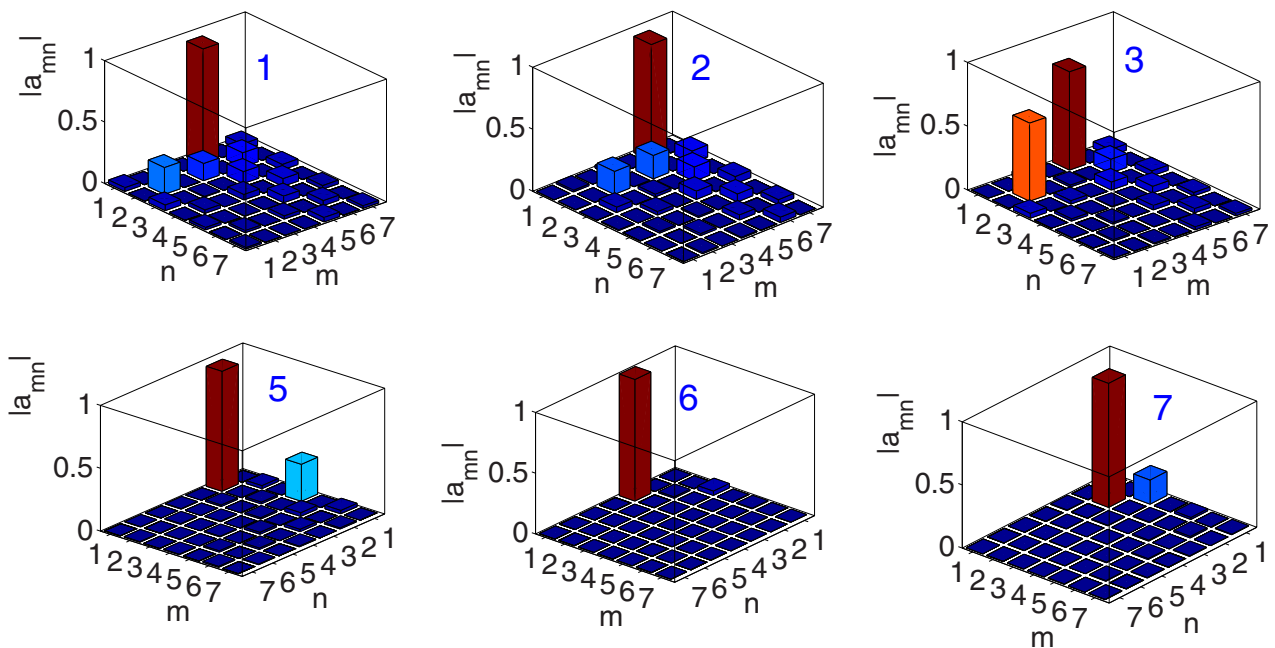


Figure 9. Expansion of BSC functions shown in figure 8 over the bridge eigenfunctions (5).

Turning back to the double-bent waveguides the symmetry arguments by Robnik are not valid because the coupling of some bridge state with the first channel can be cancelled only accidentally. The numerics show that it only occurs for the Fermi energy above the second channel threshold $4\pi^2$ as shown in figure 7(a). The reason is clear and can be readily

seen from equation (8). For the coupling matrix element (8) to be equal to zero it is necessary that the wave function of the bridge $\phi_m(x)$ had a nodal point at $x = 1/2$ (see inset figure 6). That obviously corresponds to the second channel transmission as shown in figure 7(a) by red closed circles. Therefore the BSC at $V_g < 0$ are realized through the Friedrich–Wintgen

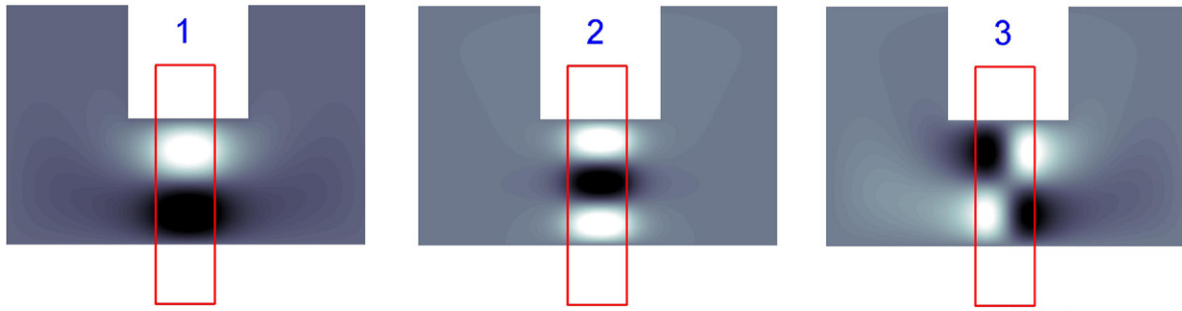


Figure 10. BSC functions for the Π -shaped waveguide with $L = 3$ labelled in figure 5(b). (1) $E = 17.24$, $V_g = -35.86$, (2) $E = 16.86$, $V_g = -90.58$, (4) $E = 29.81$, $V_g = -76.49$.

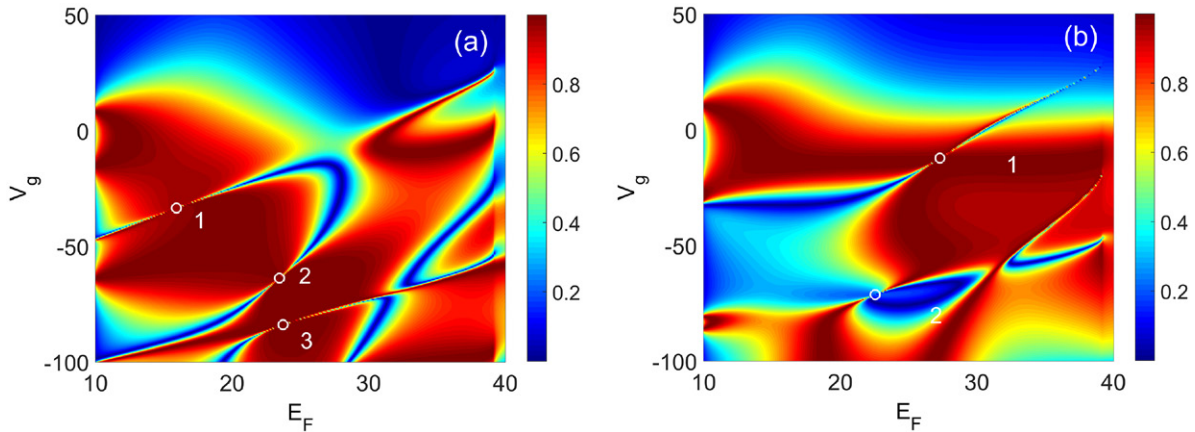


Figure 11. Conductance of double-bend waveguide versus Fermi energy and V_g for Z- (a) and Π -shaped waveguides (b) for $L = 2$. Open circles mark BSCs.

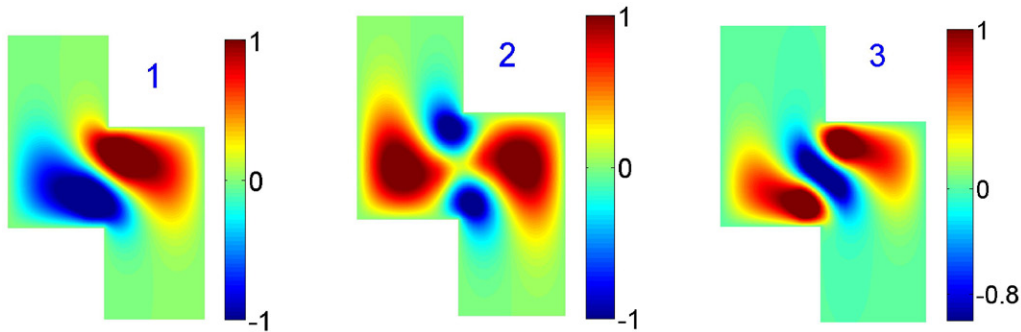


Figure 12. BSC functions for the Z-shaped waveguide labelled in figure 11(a). (1) $E = 15.9213$, $V_g = -33.54$, (2) $E = 23.464$, $V_g = -63.75$, (3) $E = 23.73$, $V_g = -83.932$.

interference mechanism. In figure 9 we show the coefficients $a_{m,n}$ of the modal expansion of the BSC wave function $\psi_{\text{BSC}}(x, y)$ over the eigenfunctions of the bridge $\psi_{m,n}(x, y)$ equation (5)

$$\psi_{\text{BSC}}(x, y) = \sum_{m,n=1} a_{m,n} \psi_{m,n}(x, y). \quad (15)$$

As seen from figures 8 and 9 the bridge wave function with longitudinal quantum number $m = 1$ dominates in BSC functions 5 and 6. For the corresponding finger gate potentials given in the figure caption these functions are mostly localized underneath the gate and decay exponentially in the waveguides. Therefore the contributions of the other bridge

states to decouple the resonant state from the first propagation channel has to be also exponentially small as seen from figure 9 for BSCs 5 and 6.

The BSC functions in the Π -shaped waveguide are shown in figure 10. For $L = 3$ and the chosen range of the finger gate potential the Π -shaped waveguide does not display the FPR type of the BSCs. Nevertheless the FPR type BSCs occur for $L = 5$. Finally in figure 11 we show the conductance of the shortest double-bend waveguides $L = 2$ with the corresponding BSCs in figure 12 for the Z-shaped waveguide and figure 14 for the Π -shaped waveguide, respectively. Figure 13 shows the coefficients of the modal expansion of the BSCs in the Z waveguide with $L = 2$ over the eigenfunctions of the

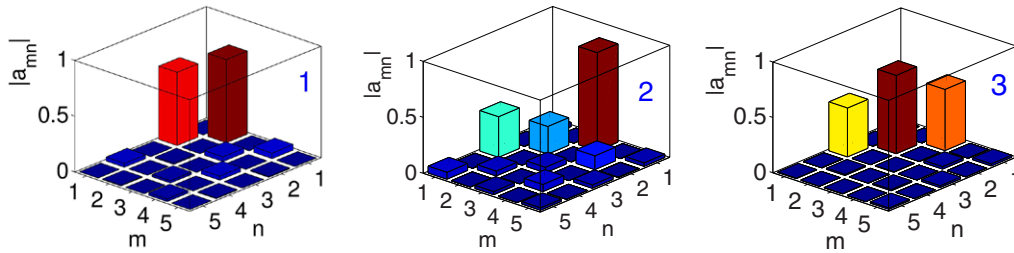


Figure 13. Expansion of BSC functions in Z-shaped waveguide shown in figure 12 over the inner eigenfunctions (5).

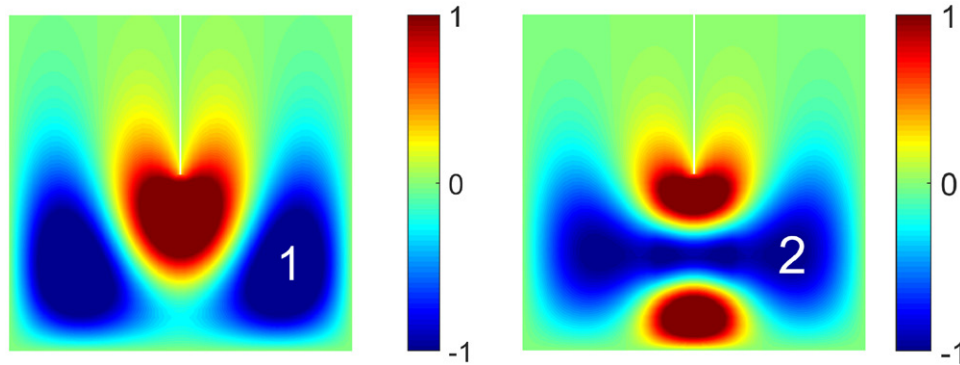


Figure 14. BSC functions for the Π -shaped waveguide labelled in figure 11(b). (1) $E = 27.3, V_g = -12.31$, (2) $E = 22.55, V_g = -71.34$.

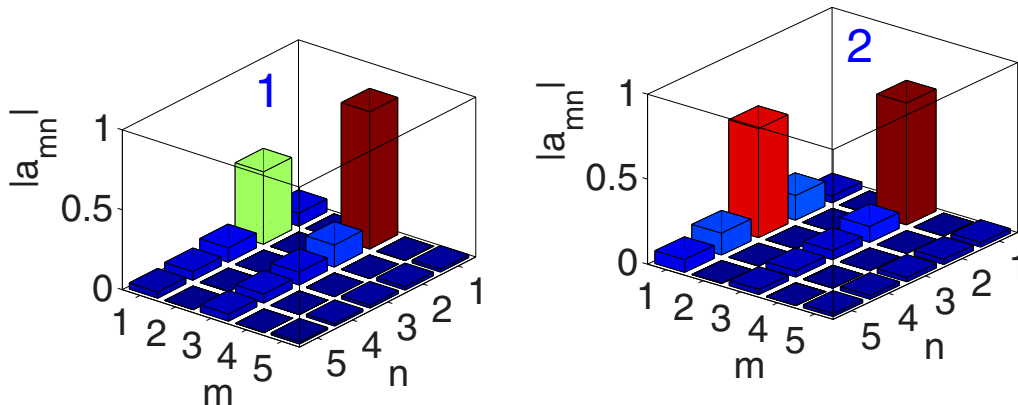


Figure 15. Expansion of BSC functions in Π -shaped waveguide shown in figure 14 over the eigenfunctions (5).

bridge $\psi_{mn}(x, y)$. One can see that only the first BSC can be approximately described by the Friedrich–Wintgen two-level approach. Similar expansions for the BSC in the Π -shaped waveguide shown in figure 15 demonstrate that the two-level approximation is applicable. Moreover one can see that only the eigenfunctions $\phi_m(x)$ symmetrical in the x -axis participate in the BSC which complies the symmetry of the waveguide.

4. Summary

We considered electron transmission in two types of double-bend waveguides, namely Z- and Π -shaped waveguides. The waveguides differ in the sequence of the chirality of the bends. In the Π -shaped waveguide the bends have the same chirality with respect to the direction of the flow, while in Z-shaped waveguide the bends have opposite chirality. It is

demonstrated that because of the difference in chirality the vortices near the bends have different current circulation. That explains the difference in conductance in those two types of waveguide. Alternatively, the origin of resonant peaks in the double-bend waveguides is explained through the approach of the effective non-Hermitian Hamiltonian. It is shown that although the central element (bridge) in both types of waveguide is identical the difference in conductance arises from the structure of the coupling matrix (8) which accounts for the coupling between the bridge and attached waveguides. Moreover the effective Hamiltonian approach with the coupling matrix (8) explains narrowing of resonant peaks with enlarging of the bridge length L . The central result of the paper, however, is the electron localization between the bends thanks to bound states in the continuum (BSC) with discrete energies embedded in the propagation band of the waveguide. The BSCs like those in figures 8, 10, 12, and 14 are shown

to be generic to both Z- and Π -shaped waveguides subject to the static potential of a finger gate. Such double-bend waveguide could be seen as a transistor with the finger gate voltage controlling the conductance as well as the resonant widths. It is shown that the finger gate potential can tune the resonant widths to zero as a result of variation of the coupling constants between the eigenstates of the bridge and the first channel continuum. Although it is hardly possible to visualize electron BSCs in microelectronics, they can be registered as singularities in the conductance where the collapse of Fano resonances occurs as shown in figures 7 and 11. Such features were experimentally observed by Lepetit *et al* [27, 28] for a dielectric resonator positioned in a microwave waveguide. We speculate that employing the equivalence between quantum waveguides and microwave systems with TM electromagnetic modes [15] it could be possible to directly observe the BSCs in microwave double-bend waveguides.

Acknowledgments

This work is supported by the Russian Science Foundation through Grant No.14-12-00266. AS is grateful K-F Berggren for discussions.

References

- [1] Weisshaar A, Lary J, Goodnick S M and Tripathi V K 1989 *Appl. Phys. Lett.* **55** 2114
- [2] Wu J C, Wybourne M N, Yindeepol M, Weisshaar A and Goodnick S M 1991 *Appl. Phys. Lett.* **59** 102
- [3] Vacek K, Okiji A and Kasai H 1993 *Phys. Rev. B* **47** 3695
- [4] Wang C-K, Berggren K-F and Ji Z-L 1995 *J. Appl. Phys.* **77** 2564
- [5] Mekis A, Chen J C, Kurland I, Fan S, Villeneuve P R and Joannopoulos J D 1996 *Phys. Rev. Lett.* **77** 3787
- [6] Carini J P, Londergan J T, Murdock D P, Trinkle D and Yung S C 1997 *Phys. Rev. B* **55** 9842
- [7] Shi Q W, Zhou J and Wu M W 2004 *Appl. Phys. Lett.* **86** 2547
- [8] Ming Y, Wang Z and Ding Z 2006 *Phys. Lett. A* **305** 302
- [9] Shevchenko S N and Kolesnichenko Ya A 2001 *JETP* **92** 811–5
- [10] Sols F and Macucci M 1990 *Phys. Rev. B* **41** 11887
- [11] Goodnick S M, Weisshaar A, Ecker A and Tripathi V K 1994 Quantum waveguide structures and devices *Workshop on (IEEE) Physics and Computation 1994 PhysComp'94 Proc.* pp 169–76
- [12] Kawamura I and Lebarton J P 1993 *J. Appl. Phys.* **73** 3577
- [13] Sokolov V V and Zelevinsky V G 1989 *Nucl. Phys. A* **504** 562
- [14] Rotter I 1991 *Rep. Prog. Phys.* **54** 635
- [15] St H -J 1999 *Quantum Chaos: An Introduction* (Cambridge: Cambridge University Press)
- [16] Alhassid Y 2000 *Rev. Mod. Phys.* **72** 895
- [17] Pichugin K, Schanz H and Seba P 2001 *Phys. Rev. E* **64** 056227
- [18] Sadreev A F and Rotter I 2003 *J. Phys. A* **36** 11413
- [19] von Neumann J and Wigner E 1929 *Phys. Z.* **30** 465
- [20] Friedrich E and Wintgen D 1985 *Phys. Rev. A* **32** 3231
- [21] Nöckel J U 1992 *Phys. Rev. B* **46** 15348
- [22] Volya A and Zelevinsky V 2003 *Phys. Rev. C* **67** 054322
- [23] Sadreev A F, Bulgakov E N and Rotter I 2006 *Phys. Rev. B* **73** 235342
- [24] Shipman S P and Venakides S 2005 *Phys. Rev. E* **71** 026611
- [25] Marinica D C, Borisov A G and Shabanov S V 2008 *Phys. Rev. Lett.* **100** 183902
- [26] Bulgakov E N and Sadreev A F 2008 *Phys. Rev. B* **78** 075105
- [27] Lepetit T, Akmansoy E, Ganne J-P and Lourtioz J-M 2010 *Phys. Rev. B* **82** 195307
- [28] Lepetit T and Kanté B 2014 *Phys. Rev. B* **90** 241103
- [29] Plotnik Y *et al* 2011 *Phys. Rev. Lett.* **107** 183901
- [30] Corrielli G, Della Valle G, Crespi A, Osellame R and Longhi S 2013 *Phys. Rev. Lett.* **111** 220403
- [31] Weimann S *et al* 2013 *Phys. Rev. Lett.* **111** 240403
- [32] Hsu C W *et al* 2013 *Light: Sci. Appl.* **2** 1
- [33] Hsu C W, Zhen B, Lee J, Chua S-L, Johnson S G, Joannopoulos J D and Soljačić M 2013 *Nature* **499** 188
- [34] Robnik M 1986 *J. Phys. A: Math. Gen.* **19** 3845
- [35] Davies J H, Larkin I A and Sukhorukov E V 1995 *J. Appl. Phys.* **77** 4504
- [36] Sadreev A F and Sherman E Ya 2013 *Phys. Rev. B* **88** 115302
- [37] Feshbach H 1958 *Ann. Phys.* **5** 357
- [38] Feshbach H 1962 *Ann. Phys.* **19** 287
- [39] Dittes F M 2000 *Phys. Rep.* **339** 215
- [40] Savin D V, Sokolov V V and Sommers H-J 2003 *Phys. Rev. E* **67** 026215
- [41] Datta S 1995 *Electronic Transport in Mesoscopic Systems* (Cambridge: Cambridge University Press)
- [42] Ando T 1991 *Phys. Rev. B* **44** 8017
- [43] Berggren K-F and Ji Z-L 1993 *Phys. Rev. B* **47** 6390
- [44] Iskra W, Rotter I and Dittes F-M 1993 *Phys. Rev. C* **47** 1086
- [45] Müller M, Dittes F-M, Iskra W and Rotter I 1995 *Phys. Rev. E* **52** 5961
- [46] Bulgakov E N, Pichugin K N, Sadreev A F and Rotter I 2006 *JETP Lett.* **84** 508
- [47] Bulgakov E N, Rotter I and Sadreev A F 2007 *Phys. Rev. A* **75** 067401
- [48] Kim C S, Satanin A M, Joe Y S and Cosby R M 1999 *Phys. Rev. B* **60** 10962
- [49] Pursey D L and Weber T A 1995 *Phys. Rev. A* **52** 3932
- [50] Ordonez G, Na K and Kim S 2006 *Phys. Rev. A* **73** 022113
- [51] Cattapan G, Lotti P 2007 *Eur. Phys. J. B* **60** 51
- [52] Cattapan G and Lotti P 2007 *Eur. Phys. J. B* **66** 517
- [53] Nakamura H, Hatano N, Garmon S and Petrosky T 2007 *Phys. Rev. Lett.* **99** 210404
- [54] Lee H and Reichl L E 2009 *Phys. Rev. B* **79** 193305
- [55] Hein S, Koch W and Nannen L 2012 *J. Fluid Mech.* **692** 257